Role of Channel Inversion in Ambient Degradation of Phosphorene FETs

Jeevesh Kumar, *Graduate Student Member, IEEE*, Utpreksh Patbhaje, and Mayank Shrivastava, *Senior Member, IEEE*

***Abstract*— Phosphorene is a potential material to replace silicon in next-generation electronic devices. However, the material is not favorable for device applications due to its gradual degradation when exposed to ambient environmental conditions. The degradation process is mainly initiated by oxygen molecules, which attacks the lone pair of phosphorus atoms. We show that in the case of phosphorene-based field-effect transistors (FETs), the channel degradation due to oxygen molecules is also influenced by the presence of channel inversion or excess (inversion) carriers. Our study reveals a unique reliability issue related to phosphorene FETs. Here, we investigate the role of channel excess holes (due to inversion) in the phosphorene degradation using the first-principles molecular dynamics computations and electrical and Raman characterization. The results show that phosphorene degrades faster under negative gate bias (excess hole) than pristine conditions (unbiased). The rapid degradation is mainly due to the enhanced chemical interaction of oxygen with the available hole in the channel. Using electrical and Raman characterization, the computational findings are experimentally verified over phosphorene FETs. The devices show a faster change in drain current and fast decay of Raman peaks in the ambient environment under negative gate bias compared to no gate bias condition. Therefore, phosphorene has an additional ambient reliability issue once exposed with negative biased during its FETs applications.**

***Index Terms*— Degradation, density functional theory (DFT), electrical characterization, phosphorene, QuantumATK, Raman.**

I. Introduction

PHOSPHORENE has many features to be a next-generation material for electronic and optoelectronic applications, mainly due to high hole mobility, a wide range of direct bandgap, and anisotropic electrical and thermal conductivity [1]–[3]. However, the material is unsuitable for the device application due to its spontaneous degradation in the ambient environment [4]–[10]. Atomic-level investigations revealed that oxygen is the primary stakeholder in determining degradation dynamics and surface chemistry in the ambient environment. Ziletti *et al.* [11] studied possible oxygen orientation and oxidation path over phosphorene surface using the density functional theory (DFT). Eslamibidgoli *et al.* [12] explored hydrophobic to the hydrophilic conversion of phosphorene surface after oxidation based on their molecular dynamics (MD) investigations. Wang *et al.* [13] predicted that phosphorene degrades via oxidation followed by surface oxide etching by water. These studies exposed the ambient degradation reliability issue of phosphorene. However, the studies do not give additional degradation reliability insights once the material is exposed to an ambient environment under external bias during its field-effect transistors (FETs) applications. Kumar *et al.* [14] explored that oxygen dissociates near the lone pair of the phosphorene, and phosphorus oxygen bonding capabilities determine the corresponding activation energy barrier. These bonding capabilities can be influenced further by the surrounding of the phosphorus atoms, especially in the presence of carrier concentrations such as excess holes or electrons. Thus, the excess carrier concentration in the devices' channels can alter ambient degradation kinetics of the phosphorene FETs. Therefore, it is worth investigating ambient degradation mechanism of the phosphorene devices under its channel inversion to understand additional degradation reliability concerns.

Here, we discuss the role of channel inversion over phosphorene surface oxidation (degradation) and its further impact using DFT and first-principles MD computations. In addition, the computational results are verified by electrical and Raman characterization of the phosphorene devices. This article starts with the MD simulation of oxygen over phosphorene surface in different doping conditions, followed by the influence of oxygen partial pressure (concentration) in the degradation process. After that, it explains degradation dynamics under different hole concentrations. Consequently, this article reveals p-type doping of phosphorene by oxygen due to surface oxidation. Finally, the work throws light on the experimental verification of the computed results by electrical and Raman probing of the phosphorene FETs in ambient conditions.

II. Computational and Experimental Details

All the computational works were done using QuantumATK simulation package [15], [16] over $5 \times 1 \times 5$ and $8 \times 1 \times 6$

Manuscript received January 31, 2022; revised March 22, 2022; accepted April 22, 2022. Date of publication May 9, 2022; date of current version May 24, 2022. This work was supported in part by the Council of Scientific and Industrial Research, India, and in part by the Defence Research and Development Organisation, India, Ministry of Electronics and Information Technology, Government of India, and in part by the Department of Science and Technology, Government of India. The review of this article was arranged by Editor J. Guo. *(Corresponding author: Jeevesh Kumar.)*

The authors are with the Department of Electronic Systems Engineering, Indian Institute of Science, Bengaluru 560012, India (e-mail: jeevesh@iisc.ac.in; mayank@iisc.ac.in).

Color versions of one or more figures in this article are available at https://doi.org/10.1109/TED.2022.3171504.

Digital Object Identifier 10.1109/TED.2022.3171504

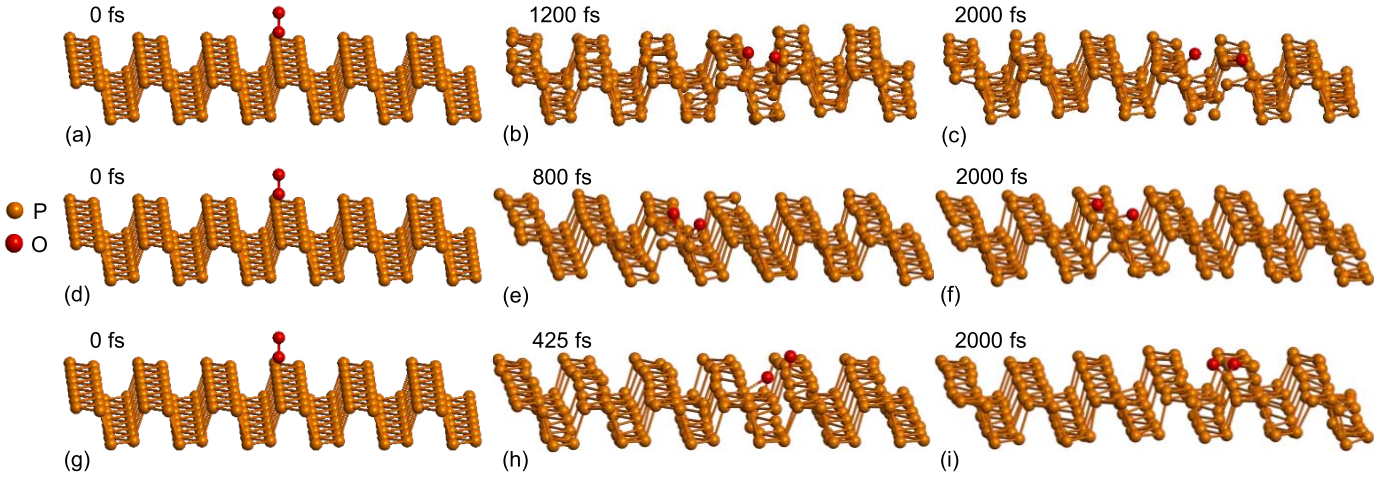

Fig. 1. Status of O_2 molecule over (a)–(c) pristine, (d)–(f) n-type doped, and (g)–(i) p-type doped phosphorene in different timestamps during MD progress.

supercells modules for only DFT [17] and first-principles MD (DFT+MD) [13] simulations, respectively. For MD, NPT (constant temperature and pressure) ensemble was used in the simulations to replicate general environmental conditions. The NPT Martyna Tobias Klein [18] algorithm was used in the calculations, which had 1-fs calculations timestamp and 100 and 500 fs of thermostat and barostat timescales, respectively. The DFT method was used to calculate the potential profile in each MD timestamp cycle. The calculations were done at 300 K, where the initial velocity of the atoms follows the Maxwell–Boltzmann distribution at the given temperature. For DFT, energy optimizations were done with 0.01-eV/Å force and 0.001-eV/Å energy tolerances. Perdew–Burke–Ernzerhof (PBE) form of generalized gradient approximation (GGA) [19] functional was used in the computation with $5 \times 1 \times 5$ k point sampling for all the modules. Grimme-D2 Van der Waals (vdW) correction [20] was considered in the calculations to capture long-range vdW interactions. Enough vacuum space (20–30 Å) was added in all the supercells to avoid interlayer wave function interaction during periodic boundary conditions.

Using standard blue tape exfoliation, back-gated phosphorene FETs were fabricated on a p-type SiO_2/Si (90 nm) substrate. Immediately after exfoliation under an N_2 rich environment, the dies were passivated under bilayer PMMA and baked for further processing [21]. Few layer phosphorene flakes were identified based on optical contrast and Raman characteristics. Evaporated Ni/Au (5/50 nm) was used as the contact metal for all the devices. E-beam lithography was used for the device fabrication process with PMMA as the resist. All the electrical measurements were done using Keithley 4200 instrumental setups, and backscattering Raman measurements were done using Horiba Labram HR with a 532-nm laser source.

III. Results and Discussion

Phosphorene degrades spontaneously once exposed to an ambient environment. Kumar *et al.* [14] explored that spontaneous degradation is mainly due to the interaction of oxygen with lone pair of phosphorus atoms. The span of the phosphorus's lone pair can be perturbed further once the material comes under external potential. Thus, the behavior of the lone pair toward oxygen is not the same when the phosphorene channel is inverted (electrostatic doping) by some external biasing in the material. MD of phosphorene degradation was captured until 2000 fs in 1-fs timestamp at 300 K in the presence of oxygen under different doping conditions (Fig. 1) for further investigations. The simulation incorporated the electrostatic doping conditions by adding external potential in the DFT+MD calculations [22]. The external potential in the analysis is equivalent to applied gate voltage in the phosphorene FET. Positive gate voltage makes the FET's channel n-type equivalent to negative external potential in the computational model. Similarly, negative gate voltage, which makes the channel p-type, is equivalent to positive external potential in the model. Hereafter, p-/n-type doping mentioned in this article means assimilation of negative/positive external potential in the corresponding calculations.

A. Degradation Dynamics Under Excess Carriers

Phosphorene degrades faster in p-type doping than pristine and n-type doping under similar conditions. The oxygen molecule dissociates after 425 fs when phosphorene is p-type doped [Fig. 1(g)–(i)]. On the other hand, the dissociation takes place after 800 and 1200 fs in the n-type [Fig. 1(d)–(f)] and pristine [Fig. 1(a)–(c)] condition, respectively.

The p-type doping in phosphorene gives excess holes inside the system. The excess hole is equivalent to the availability of vacant orbitals, which can attract electrons quickly once they come around its bonding regimes. When oxygen approaches the phosphorus atom, its dissociated atoms bond quickly to the adjacent phosphorus atom due to the interaction of its lone pairs to available vacant orbitals (holes) in the phosphorene. Thus, the available hole catalyzes oxygen dissociation over phosphorene and boosts the reaction process. Total energy evolution of the system during MD progress [Fig. 2(a)] reflects

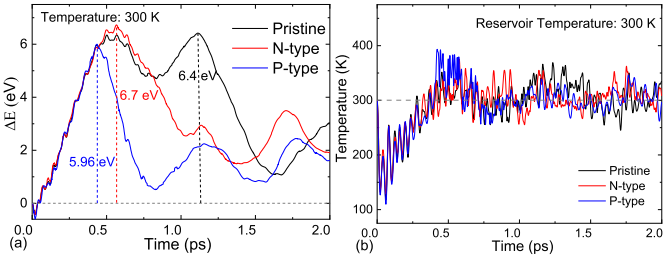

Fig. 2. (a) MD energy change and (b) corresponding temperature profiles comparison of the phosphorene degradation in pristine, n-type, and p-type conditions.

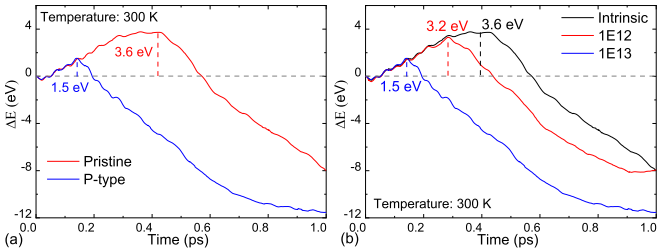

Fig. 3. (a) MD change in energy comparison of phosphorene + five oxygen system in (a) pristine and p-type doping condition and (b) different p-type doping concentration.

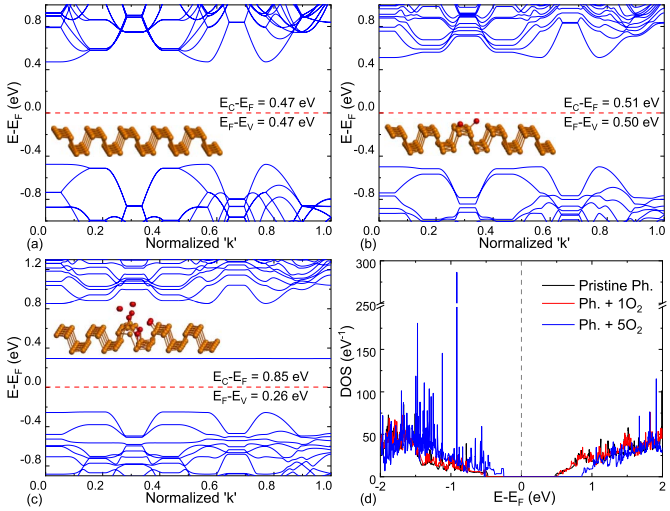

Fig. 4. Band structure of a $5 \times 1 \times 5$ supercell of (a) pristine phosphorene, (b) phosphorene with an oxygen molecule, and (c) phosphorene with five oxygen molecules. Normalized "*k*" is along $Y \rightarrow G \rightarrow X \rightarrow S \rightarrow R \rightarrow U \rightarrow X \rightarrow S \rightarrow Y \rightarrow T \rightarrow Z \rightarrow G \rightarrow U \rightarrow Z$. Position of *Y*, *G*, *X*, *S*, *R*, *U*, *X*, *S*, *Y*, *T*, *Z*, *G*, *U*, and *Z* points on the *k* axis are 0, 0.05, 0.15, 0.21, 0.28, 0.34, 0.41, 0.46, 0.57, 0.64, 0.70, 0.77, 0.90, and 1.0, respectively. (d) Density of states (DOS) plot of all the three modules. Fermi energy is at zero energy level in all the band structures and DOS plots.

that the degradation of p-type phosphorene has less activation energy (5.96 eV) compared to pristine (6.4 eV) and n-type doping (6.7 eV). The system crosses its activation barrier early in the reaction and releases extra energy quickly, a signature of rapid bond formation. The released energy raises system temperature temporarily before transferring into the reservoir [Fig. 2(b)].

On the other hand, pristine and n-type-doped phosphorene have similar activation energy. Available excess electrons in n-type phosphorene can drive the oxidation process and overcome the activation barrier early compared to its pristine counterpart [23]. However, the activation barrier height or total energy of the reaction does not change significantly like p-type phosphorene.

B. Hole-Assisted Rapid Degradation

Excess hole in phosphorene captivates oxygen toward its surface, making the degradation faster than pristine or excess electron. Besides, phosphorene is a more promising material for its high hole mobility than electron mobility [3]. The material does not show significant n-type current compared to p-type current in similar conditions. Thus, it is worth further investigating phosphorene FETs' ambient degradation reliability issues under excess hole concentration (negative gate biasing).

The computations were repeated with increased oxygen partial pressure (five O_2 in the supercell) for a better/realistic model. Their dynamics and corresponding energy evolution profiles [Fig. 3(a)] reflect that p-type doping reduces the activation energy significantly (3.6–1.5 eV) and hence causes rapid phosphorene-oxygen interactions compared to its pristine counterpart. The processes were exothermic and therefore had lesser activation energies from the corresponding mono oxygen dissociation processes. Thus, phosphorene degrades spontaneously in both conditions. However, the degradation rate is faster for p-type doping than pristine one.

The p-type-assisted degradation is further verified by changing the electrostatic hole doping concentration in the phosphorene. Once doping concentration is reduced, the activation energy of the process is increased, which slows down the degradation mechanism in the phosphorene [Fig. 3(b)]. Therefore, it is confirmed that the phosphorene degradation mechanism in the ambient environment is fast when it is negatively biased (p-type doped) compared to an unbiased condition.

C. Oxygen-Assisted p-Type Doping

Once phosphorene is kept in the ambient environment, it interacts with oxygen and makes corresponding surface oxides. The surface oxygen changes phosphorene's channel from intrinsic to p-type. Band structure and density of states (DOS) comparison of pristine and oxidized phosphorene give the doping signature after oxidation (Fig. 4). The Fermi energy level of the system moves near the valence band maxima (VBM) once oxygen comes over the phosphorene surface.

The p-type doping is mainly due to charge (electron) transfer from phosphorene to oxygen during oxidation. Mulliken electron population around the bonded oxygen atoms [1–6 in Fig. 5(a)] and the corresponding bonded phosphorus atoms show that oxygen/phosphorous gains/losses the total number of electrons (average) after the oxidation process [Fig. 5(b)]. Thus, electrons drift from phosphorene toward bonded oxygen, which leads to the Fermi level moving near the valence band.

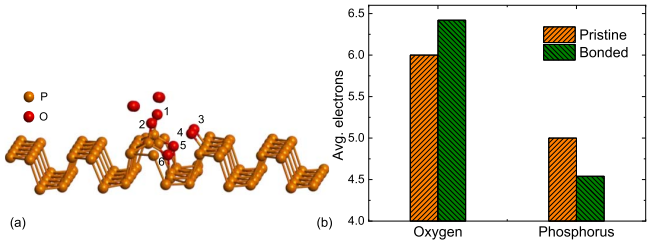

Fig. 5. (a) Energy optimized a 5 × 1 × 5 supercell of phosphorene with five oxygen molecules. (b) Comparison of average valence electrons of bonded oxygen atoms (1–6) and corresponding phosphorus atoms with their valence electrons in pristine conditions.

D. Experimental Validation Over Phosphorene FETs

P-type doping of phosphorene during its degradation process can be a parameter to investigate the degradation rate. The doping makes the phosphorene (few layer black phosphorous) FET more conductive with time progress until the exposed layer is significantly oxidized. Thus, when phosphorene FET is under negative gate bias in ambient conditions, its transfer characteristics (I_d–V_g) shifts right due to p-type doping. Therefore, output characteristics (I_d–V_d) of the FET gradually move upward with time when phosphorene degrades at a given negative gate biased.

Few layer phosphorene FETs [Fig. 6(a)] were processed by standard micromechanical cleavage (exfoliation) methods. Three intensity peaks (A^1_g, B_{2g}, and A^2_g) along with silicon peak [Fig. 6(b)] in the backscattering Raman measurement of the exfoliated flake confirm that the material is a few layer phosphorene [24]. The I_d–V_g and I_d–V_d characteristics [Fig. 6(c) and (d)] reflect that the FET has decent gate control and ohmic contacts. Usually, double sweep data are incorporated in the transfer characteristics. However, long time stress can impact the device performance, especially under ambient degradation. We tried to minimize S-D stress time in the devices to mitigate the stress effect, captured only single sweep data in the experiments.

Two phosphorene devices were characterized in the ambient environment to verify the role of negative gate biases over degradation. The I_{ds}–V_{ds} of the devices were measured in 2-min intervals at −40-V gate biases. In the first condition, the devices were in floating states between the consecutive measurement (floating device). On the other condition, the devices were continued to be under negative biased (V_{gs} = −40 V) between the consecutive measurement (biased device). Both the devices show the drain current increment rate at given drain voltage is faster under negative biases [Fig. 7(b) and (d)] than under floating conditions [Fig. 7(a) and (c)]. As explored using computations, phosphorene degrades spontaneously in a floating condition also. However, it was captured in device 1 only, probably due to a relatively high reaction rate than device 2 because of different surface profiles. Interestingly, I_{ds} drops from 0 to 2 min in device 2 under negative bias [Fig. 7(d)]. The discrepancy could be due to device variability, experimental artifact, or existing surface oxide etching. Actually, oxygen and water are both involved in the degradation process of phosphorene [4], [5], [14]. The process initiates with surface

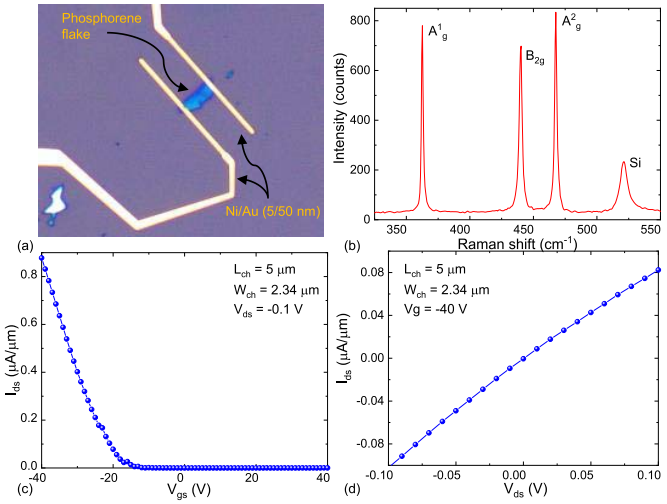

Fig. 6. (a) Optical image of the fabricated phosphorene device. (b) Raman scattering peaks of the flake. (c) I_{ds}–V_{gs} and (d) I_{ds}–V_{ds} of the fabricated device.

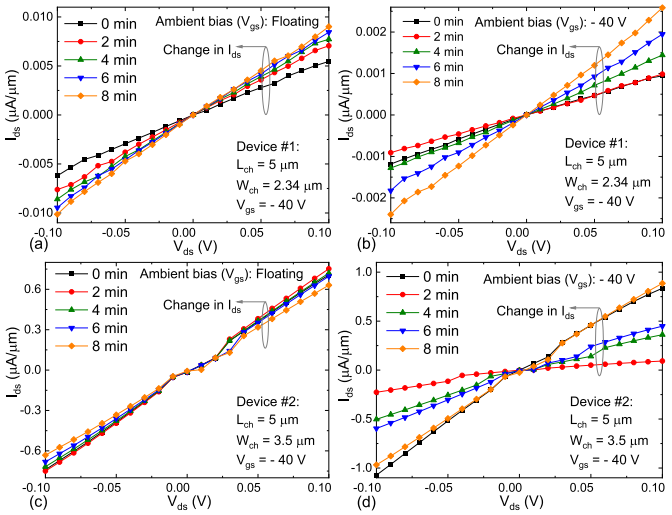

Fig. 7. I_d–V_d characteristics of the devices at a different time in (a) and (c) floating ambient biased and (b) and (d) negative ambient biased conditions.

oxidation by oxygen molecules followed by the surface oxide etching by water molecules. Due to doping, a rise in drain current (I_{ds}) is expected during the oxidation process. During oxide etching, we can expect a decrement in I_{ds}. In device 2, I_{ds} increases consistently from 2 to 8 min due to doping. The drop between 0 and 2 min can be due to existing surface oxide etching assisted by heat generation during the first measurement (0 min). In fact, device 1 also reflects a similar signature as I_{ds} at 0 and 2 min is almost the same [Fig. 7(b)]. Here, the initial current drop due to oxide etching is almost recovered by doping due to further surface oxidation. The increment in the drain current resembles hole doping due to phosphorene degradation (oxidation), as observed computationally (Fig. 4). Therefore, it is clear that phosphorene degrades faster under negative gate bias than under floating conditions.

Raman characteristics also show fast degradation of phosphorene under negative gate bias than floating conditions.

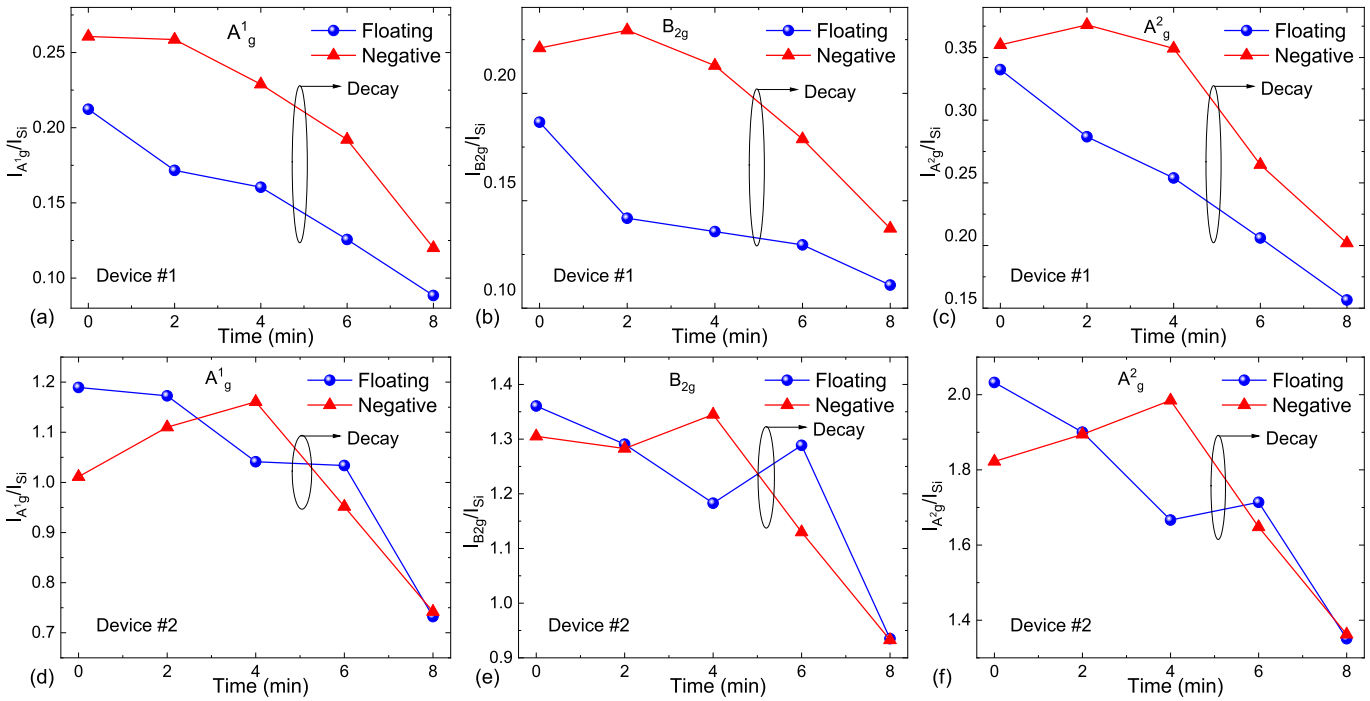

Fig. 8. Phosphorene Raman intensity peaks, normalized by silicon peaks, under floating and negative ($V_{ds} = -40$ V) gate bias. (a) and (d) A^1_g, (b) and (e) B_{2g}, and (c) and (f) A^2_g.

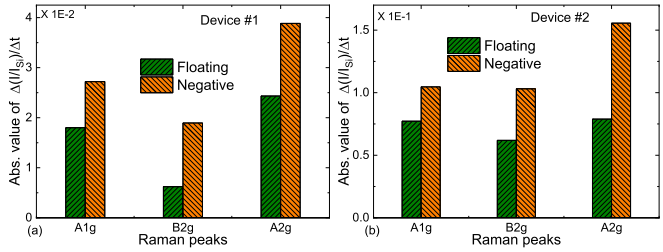

Fig. 9. Average rate of change of intensity ratio ($\Delta(I/I_{Si})/\Delta t$) during 4–8 min. (a) Device 1, (b) Device 2. All the peaks have a higher rate of change under negative bias than floating for both the devices.

Usually, the intensity of phosphorene's Raman modes, normalized with silicon peak, decreases with time during degradation [25]. Thus, the degradation rate under floating and negative bias can be compared using the rate of change of their Raman's peak intensity ratios (I/I_{Si}) with time. A higher rate of change in I/I_{Si} (slope) reflects the faster rate of degradation. The processed devices were probed under the Raman system in floating and negative gate-biased conditions. All the intensity peaks (A^1_g, B_{2g}, and A^2_g) show sharp decay, after initial increments, under negative gate biased than floating condition (Fig. 8). The devices were observed under negative gate biased followed by floating biased. Thus, probable causes of initial peaks rise under negative gate bias (0–4 min) are optical interference and/or [21] laser annealing and surface oxide etching of the phosphorene. In the later phase (4–8 min), the average slope ($\Delta(I/I_{Si})/\Delta t$) of peak ratios under negative bias dominates over the floating condition for both the devices (Fig. 9), which reflects faster degradation under negative bias conditions.

Based on the Raman characterization, Kumar *et al.* [8] commented that phosphorene has faster degradation under floating conditions than negative gate bias. However, the authors only probed the degradation for a couple of seconds. The present analysis consists of a detailed investigation of the phosphorene FET's reliability, computationally and experimentally. The investigation says that such a short-time Raman probing is not enough to capture the actual degradation behavior of the phosphorene.

Therefore, based on electrical and Raman observation, we can confirm that phosphorene degrades faster under negative gate biased than floating conditions, as explored in the MD investigations.

IV. Conclusion

In summary, we explored the ambient degradation mechanism of phosphorene under floating and negative biased (electrostatic doping) conditions using the first-principle MD simulations and electrical and Raman characterization. The investigations reveal that phosphorene degrades spontaneously in all the biasing conditions. However, the degradation rate is faster in excess holes under negative gate biases than in pristine conditions. The degradation rate was enhanced further by increasing inversion hole concentration (by negative gate biasing) in the channel. Besides, the oxidation process dopes the phosphorene from intrinsic to p-type due to charge (electron) transfer from phosphorous to oxygen. Finally, we verified the fast degradation of phosphorene FETs by their electrical and Raman characteristics. Phosphorene FETs show a significant increment in the drain current under negative ambient bias compared to floating conditions. Furthermore, normalized

Raman peaks decay faster under negative gate voltage. The electrical and Raman characteristics are consistent with our computational findings, showing rapid ambient degradation of phosphorene devices in the presence of inversion holes. These findings can help understand additional ambient reliability concerns once phosphorene is used for FET applications.

ACKNOWLEDGMENT

The authors would like to thank the NNetRA Program of MeitY, DST, and MHRD Government of India, as well as DRDO and CSIR, for supporting this work.

REFERENCES

[1] L. Li *et al.*, "Black phosphorus field-effect transistors," *Nature Nanotechnol.*, vol. 9, no. 5, pp. 372–377, 2014, doi: 10.1038/NNANO.2014.35.

[2] S. Das, M. Demarteau, and A. Roelofs, "Ambipolar phosphorene field effect transistor," *ACS Nano*, vol. 8, no. 11, pp. 11730–11738, Nov. 2014, doi: 10.1021/nn505868h.

[3] H. Liu, Y. Du, Y. Deng, and P. D. Ye, "Semiconducting black phosphorus: Synthesis, transport properties and electronic applications," *Chem. Soc. Rev.*, vol. 44, no. 9, pp. 2732–2743, May 2015, doi: 10.1039/C4CS00257A.

[4] Y. Huang *et al.*, "Interaction of black phosphorus with oxygen and water," *Chem. Mater.*, vol. 28, no. 22, pp. 8330–8339, Nov.2016, doi: 10.1021/acs.chemmater.6b03592.

[5] M. van Druenen *et al.*, "Evaluating the surface chemistry of black phosphorus during ambient degradation," *Langmuir*, vol. 35, no. 6, pp. 2172–2178, Feb. 2019, doi: 10.1021/acs.langmuir.8b04190.

[6] T. Zhang *et al.*, "Degradation chemistry and stabilization of exfoliated few-layer black phosphorus in water," *J. Amer. Chem. Soc.*, vol. 140, no. 24, pp. 7561–7567, Jun. 2018, doi: 10.1021/jacs.8b02156.

[7] J. Plutnar, Z. Sofer, and M. Pumera, "Products of degradation of black phosphorus in protic solvents," *ACS Nano*, vol. 12, no. 8, pp. 8390–8396, Aug. 2018, doi: 10.1021/acsnano.8b03740.

[8] J. Kumar *et al.*, "Physical insights into phosphorene transistor degradation under exposure to atmospheric conditions and electrical stress," in *Proc. IEEE Int. Rel. Phys. Symp. (IRPS)*, Apr. 2020, pp. 1–4, doi: 10.1109/IRPS45951.2020.9129123.

[9] A. E. Naclerio *et al.*, "Visualizing oxidation mechanisms in few-layered black phosphorus via *In situ* transmission electron microscopy," *ACS Appl. Mater. Interfaces*, vol. 12, no. 13, pp. 15844–15854, Apr. 2020, doi: 10.1021/acsami.9b21116.

[10] C. Hyun, J. H. Kim, J.-Y. Lee, G.-H. Lee, and K. S. Kim, "Atomic scale study of black phosphorus degradation," *RSC Adv.*, vol. 10, no. 1, pp. 350–355, Jan. 2020, doi: 10.1039/c9ra08029e.

[11] A. Ziletti, A. Carvalho, D. K. Campbell, D. F. Coker, and A. H. C. Neto, "Oxygen defects in phosphorene," *Phys. Rev. Lett.*, vol. 114, no. 4, Jan. 2015, Art. no. 046801, doi: 10.1103/PhysRevLett.114.046801.

[12] M. J. Eslamibidgoli and M. H. Eikerling, "Mechanical and chemical stability of monolayer black phosphorous studied by density functional theory simulations," *J. Phys. Chem. C*, vol. 122, no. 39, pp. 22366–22373, Oct. 2018, doi: 10.1021/acs.jpcc.8b04344.

[13] G. Wang, W. J. Slough, R. Pandey, and S. P. Karna, "Degradation of phosphorene in air: Understanding at atomic level," *2D Mater.*, vol. 3, no. 2, Apr. 2016, Art. no. 025011, doi: 10.1088/2053-1583/3/2/025011.

[14] J. Kumar and M. Shrivastava, "First-principles molecular dynamics insight into the atomic level degradation pathway of phosphorene," *ACS Omega*, vol. 7, no. 1, pp. 696–704, Jan. 2022, doi: 10.1021/acsomega.1c05353.

[15] J. M. Soler *et al.*, "The SIESTA method for *ab initio* order-N materials simulation," *J. Phys., Condens. Matter*, vol. 14, no. 11, p.2745, 2001.

[16] *QuantumATK R-2020*. Synopsys, Mountain View, CA, USA.

[17] W. Kohn and L. J. Sham, "Self–consistent equations including exchange and correlation effects," *Phys. Rev.*, vol. 140, no. 4A, pp. A1133–A1138, Nov. 1965, doi: 10.1103/PhysRev.140.A1133.

[18] G. J. Martyna, D. J. Tobias, and M. L. Klein, "Constant pressure molecular dynamics algorithms," *J. Chem. Phys.*, vol. 101, no. 5, pp. 4177–4189, 1994.

[19] J. P. Perdew, K. Burke, and M. Ernzerhof, "Generalized gradient approximation made simple," *Phys. Rev. Lett.*, vol. 77, no. 18, p. 3865, 1996.

[20] S. Grimme, "Semiempirical GGA-type density functional constructed with a long-range dispersion correction," *J. Comput. Chem.*, vol. 27, no. 15, pp. 1787–1799, Sep. 2006, doi: 10.1002/jcc.20495.

[21] F. Alsaffar *et al.*, "Raman sensitive degradation and etching dynamics of exfoliated black phosphorus," *Sci. Rep.*, vol. 7, pp. 1–9, Mar. 2017, doi: 10.1038/srep44540.

[22] B. Chakraborty *et al.*, "Electron-hole asymmetry in the electron-phonon coupling in top-gated phosphorene transistor," *2D Mater.*, vol. 3, no. 1, Feb. 2016, Art. no. 015008, doi: 10.1088/2053-1583/3/1/015008.

[23] K. L. Kuntz *et al.*, "Control of surface and edge oxidation on phosphorene," *ACS Appl. Mater. Interfaces*, vol. 9, no. 10, pp. 9126–9135, Mar. 2017, doi: 10.1021/acsami.6b16111.

[24] H. B. Ribeiro, M. A. Pimenta, and C. J. S. de Matos, "Raman spectroscopy in black phosphorus," *J. Raman Spectrosc.*, vol. 49, no. 1, pp. 76–90, Jan. 2018, doi: 10.1002/jrs.5238.

[25] A. Favron *et al.*, "Photooxidation and quantum confinement effects in exfoliated black phosphorus," *Nature Mater.*, vol. 14, no. 8, pp. 826–832, Aug. 2015, doi: 10.1038/nmat4299.